



Impact of titanium precursors on formation and electrochemical properties of $\text{Li}_4\text{Ti}_5\text{O}_{12}$ anode materials for lithium-ion batteries

Chung-Yuan Kang¹ · Marcin Krajewski² · Jeng-Yu Lin¹

Received: 22 July 2020 / Revised: 24 September 2020 / Accepted: 25 September 2020
© The Author(s) 2020

Abstract

This work describes comparative study on the application of $\text{Li}_4\text{Ti}_5\text{O}_{12}$ (LTO) as anode materials for lithium-ion batteries which were successfully prepared by sol-gel synthesis with the use of two titanium sources. One of them was anatase-type titanium dioxide (TiO_2), whereas the second was tetrabutyl titanate (TBT). Both obtained LTO materials were very similar in terms of their crystallinity and purity. In turn, the sample synthesized with TBT source revealed better particle dispersibility, and its particles were slightly lower in size. These particular features resulted in higher Li^+ diffusion coefficient and better kinetic of Li^+ ions during charge transfer reactions for the LTO synthesized with TBT source. This reflected in specific capacitance values for both electrodes which equalled 150 mAh g^{-1} , 120 mAh g^{-1} , and 63 mAh g^{-1} for TBT-LTO and 120 mAh g^{-1} , 80 mAh g^{-1} , and 58 mAh g^{-1} for TiO_2 -LTO at C-rates of 1, 5, and 10 C, respectively.

Keywords Anode material · Lithium titanate · Lithium-ion batteries · Sol-gel synthesis · Tetrabutyl titanate · Titanium dioxide

Introduction

Since the energy crisis in 1973 associated with the future predictions about the shortage of oil and other finite energy sources [1, 2], many people have begun to pay attention to the issues related to energy storage. This trend has caused that some of them look towards alternative renewable energy sources like solar energy, hydropower, wind power, and geothermal power. Nevertheless, the energy from natural sources requires the effective storage systems. This is one of the reasons why many scholars work on the energy storage devices such as lithium-ion batteries (LIBs) [3].

In recent years, the cubic spinel $\text{Li}_4\text{Ti}_5\text{O}_{12}$ (LTO) has become a promising anode material because of its many advantages, including a high working potential of the redox couple $\text{Ti}^{4+}/\text{Ti}^{3+}$ at 1.55 V (vs. Li/Li^+), high safety, good cycling stability, high energy density, and excellent Li^+ intercalation/extraction reversibility without metallic lithium deposition and with near zero volume change during discharge–charge processes [4–8]. On the other hand, the LTO has some serious drawbacks, such as low theoretical capacity (175 mAh g^{-1}), poor intrinsic electronic conductivity ($10^{-13} \text{ S cm}^{-1}$), and low lithium-ion diffusion coefficient (10^{-9} – $10^{-13} \text{ cm}^2 \text{ s}^{-1}$). Some of them still restrain possible application of the LTO as anode material in LIBs [9, 10].

So far, few strategies which aim to decrease the impact of some unwanted drawbacks and at the same time to improve the electrochemical performance of the LTO electrode material have been proposed. Among them, three are very common. The first one is to reduce the LTO particle size [11, 12]. This allows (i) enhancing the active surface area, (ii) shortening the lithium-ion transfer path, and (iii) speeding up electrochemical reaction. For instance, Michalska et al. [8] as well as Pohjalainen et al. [12] designed various milling processes in order to prepare the LTO with different sizes, and they noticed that the smaller primary particle size of material, the higher its specific capacity was. Also, Wang et al. [13] studied the LTO electrodes which were synthesized by using the TiO_2 particles

Electronic supplementary material The online version of this article (<https://doi.org/10.1007/s10008-020-04831-8>) contains supplementary material, which is available to authorized users.

✉ Marcin Krajewski
mkraj@ippt.pan.pl

✉ Jeng-Yu Lin
jylin@ttu.edu.tw

¹ Department of Chemical Engineering and Biotechnology, Tatung University, No. 40, Sec. 3, Chungshan North Rd., Taipei City 104, Taiwan

² Institute of Fundamental Technological Research, Polish Academy of Sciences, Pawińskiego Street 5B, 02-106 Warsaw, Poland

with different sizes. According to their results, the small particle size promoted the better electrochemical performance. On the other hand, they observed that the use of too small particle sizes resulted in the particle agglomeration which caused the worse electrochemical performance. The second strategy is associated with the doping of LTO material. This can be realized through cation (e.g., Nb^{5+} [7], Mg^{2+} [14], Ru^{4+} [15], V^{5+} [16], Cu^{2+} [17], Zn^{2+} [18], Fe^{3+} [19]), and non-metal anion (e.g., Br^- [20]) doping into Li, Ti, and O sites, and it usually leads to increase of electronic conductivity as well as stabilization of cycling behavior at high C-rates. The third method of LTO performance improvement is its surface modification with carbon [21–24] or other compounds (e.g., AlF_3 [25], TiN [26]). This can mainly improve the electronic conductivity of LTO electrode.

The LTO material can be successfully synthesized with various titanium sources. Among them, the anatase-type titanium dioxide (TiO_2) powder is one of the most frequently used in the direct LTO preparation [8, 13, 14, 16, 19, 21, 27, 28]. However, the anatase TiO_2 powder is sometimes prepared in an indirect way, for instance, through the leaching of hydrolyzed titania residues from natural ilmenite [29] or the decomposition of tetrabutyl titanate ($\text{Ti}(\text{OC}_4\text{H}_9)_4$; TBT) [9, 28, 30, 31]. After that, the obtained anatase powder is taken to the LTO synthesis. Taking an advantage of direct and indirect anatase sources, we have performed a simple sol-gel synthesis with two various titanium sources, i.e., titanium dioxide and tetrabutyl titanate, in order to investigate their impact on synthesis and electrochemical properties of the LTO anode materials for lithium-ion batteries. Our approach can be considered another interesting strategy which leads to the synthesis of the LTO electrode materials with various electrochemical properties.

Experimental

Synthesis of the pristine LTO by using the sol-gel method

The lithium acetate dihydrate ($\text{CH}_3\text{COOLi} \cdot 2\text{H}_2\text{O}$) (98%, Acros), titanium dioxide (98% anatase powder, Acros) or tetrabutyl titanate (TBT; 99%, Acros), and citric acid (CA; 99%, Fisher Chemical) were used as lithium source, titanium sources, and chelating agent, respectively.

In the synthesis, the proper amount of reagents with the Li:Ti:CA molar ratio of 4:5:4 was separately dissolved in 50 ml of 95% ethanol to obtain three solutions. In order to avoid lithium salt heat loss during the high-temperature calcination process, the excess of 5%_{wt.} of lithium salt was added to the lithium solution. Afterwards, the lithium solution was slowly dropped to the titanium solution with continuous stirring at room temperature overnight. This led to the formation

of a homogeneous precursor solution. Then, the precursor solution was mixed with CA and was heated at 120 °C under continuous stirring for 8 h. This caused the formation of a gel precursor which was dried at oven 60 °C for 2 days to remove the residual solvent. Finally, it was subjected to the thermal pre-treatment at 350 °C for 4 h under air atmosphere and then cooled down to room temperature. The obtained semi-product was milled by agate mortar to form homogeneous powder which was thermally treated at 800 °C for 12 h under air atmosphere to get the final LTO materials.

It should be also noted that the synthesis procedures for both LTO materials were exactly the same apart from the titanium source. Therefore, in order to differentiate both samples, we had designated them as TiO_2 -LTO and TBT-LTO.

Physical characterization of materials

The crystallinity and purity of synthesized materials were verified by powder X-ray diffraction (XRD) using the Lab XRD 6000 (Shimadzu Corporation, Japan) operating at 40 kV and 30 mA and equipped with a $\text{Cu K}\alpha$ lamp ($\lambda_{\text{XRD}} = 1.5406 \text{ \AA}$). The XRD patterns were collected in 2θ range of 10–80° with step of 0.02 degree and scan rate of 0.6 degree/min. The morphology and particle size of the prepared materials were analyzed by using a scanning electron microscope (SEM; JSM-7800F, JEOL). The particle size was also determined using a particle size analyzer (PSA; BECKMAN COULTER LS 13320). In this case, the water dispersions of both samples were used. The molecular bonding and structural properties of both LTO particles were studied using a Raman spectrometer (UniDRON in Via, $\lambda_{\text{RS}} = 532 \text{ nm}$). The specific surface areas of the investigated LTO materials were determined with the BET (Brunauer–Emmett–Teller) method based on the nitrogen adsorption–desorption measurements performed with an ASAP 2020-Micromeritics analyzer.

Electrochemical characterization

The as-prepared LTO materials as active electrode materials, acetylene black (UBIQ Technology CO.) as the conductive material, and polyvinylidene fluoride (PVDF) (Kynar HSV 900) as the binder were mixed in a weight ratio of 83:10:7 and dissolved in N-methyl-2-pyrrolidone (NMP, 99%, Alfa Aesar). After that, the mixture was continually stirred for 2 h. The resulting slurry was deposited on Cu foil (UBIQ Technology CO.) acted as a current collector. The thickness of electrode was about 15 μm . Then, the current collector covered by electrode material was dried at 120 °C for 12 h in a vacuum to remove residual solvent.

The electrochemical tests were prepared using CR2032 coin-type cell. Prior to the assembly of coin cells, the electrodes, lithium metal, and separator (Union Chemical IND. CO., LTD) were punched for a disk with a diameter 0.5 cm,

0.6 cm, and 1.8 cm, respectively. The coin cells were assembled in an argon-filled glove box. The 1.0 M LiPF₆ in ethylene carbonate (EC):diethyl carbonate (DEC) (1:1, v/v) was used as electrolyte (Formosa Plastics Corporation CO.).

The galvanostatic charge and discharge (GCD) tests were executed by a commercial battery auto test system (NEWARE CT-4000) within a cutoff voltage region of 1.0–2.5 V (vs. Li/Li⁺) at varied current densities at room temperature. The cyclic voltammetry (CV) analysis was collated at voltage of 1.0–2.5 V (vs. Li/Li⁺) at 0.1 mV s⁻¹ with VMP-300 (UBOTECH). The electrochemical impedance spectroscopy (EIS) analysis was carried out by using Zahner Zennium in the frequency range from 100 mHz to 100 kHz with the amplitude of 5 mV. The EIS measurements of the coin cells were detected after 10 cycles of CV tests.

Results and discussion

The XRD patterns of the pristine TiO₂-LTO and TBT-LTO materials prepared via a sol-gel method are shown in Fig. 1. Both investigated samples exhibit very similar XRD patterns. The main diffraction peaks in XRD patterns are located at $2\theta = 18.4^\circ$, 35.6° , 43.3° , 57.2° , and 62.9° , and those positions can be indexed to (111), (311), (400), (333), and (440) lattice planes according to JCPDS file card no. 49-0207. Furthermore, the obtained LTO materials reveal the spinel structure with the space group Fd3m. According to the XRD data, the samples are well crystalline because the well-defined sharp diffraction peaks are detected. It is also evident that both LTO materials are quite pure. Only in the case of TiO₂-LTO, low-intensity peak displayed at $2\theta = 28^\circ$ can be considered impurity which might be assigned to the Li₂Ti₃O₇ (JCPDS file card No. 40-0303) and

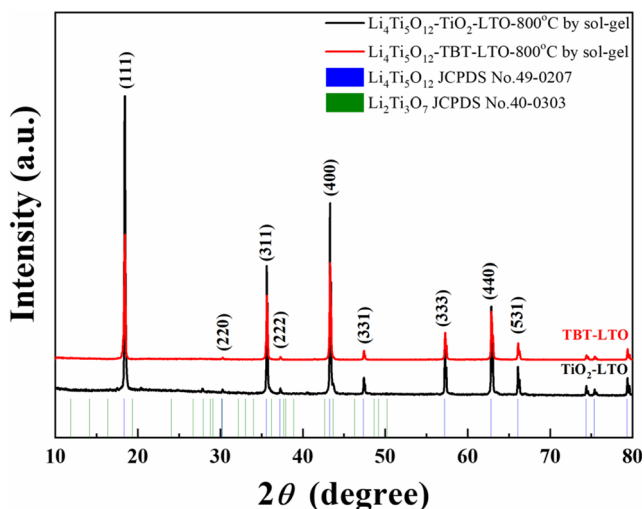


Fig. 1 XRD patterns of TiO₂-LTO and TBT-LTO prepared by using the sol-gel method

attributed to the lithium metal heat loss which occurs during the high-temperature calcination [32].

The Raman spectra for both investigated LTO materials were collected in the range of 200–2000 cm⁻¹, and they are shown in Fig. 2. In general, the positions of bands in both Raman spectra are very similar. The band located at 235 cm⁻¹ is associated with the bending vibration of the O–Ti–O. In turn, the bands at 348 cm⁻¹ and 427 cm⁻¹ correspond to the stretching–bending vibrations of the Li–O bonds in LiO₄ and LiO₆ polyhedrons. The last two bands at 679 cm⁻¹ and 750 cm⁻¹ are related to the vibrations of Ti–O bonds in TiO₆ octahedra [5, 6, 8, 21, 26]. It is also important that the intensities of bands in both Raman spectra are different. In fact, much lower intensities were recorded for the TiO₂-LTO sample. At this point, it should be underlined that the parameters of Raman measurements were exactly the same for both investigated LTO materials. Hence, it is expected that the observed differences in the intensities of Raman spectra can be explained considering the surface area of TiO₂-LTO and TBT-LTO materials which was determined with the BET method and equalled 1.49 and 2.17 m² g⁻¹, respectively. Thus, the sample with lower surface area exhibited the lower intensities of Raman signal. Concluding, the performed Raman measurements for both investigated samples revealed the typical structural features observed in the LTO material. Moreover, the lower Raman signal was observed for the LTO sample with lower surface area.

The SEM images which display the morphology of TiO₂-LTO and TBT-LTO samples are shown in Fig. 3. Comparing these images, one can see that TBT-LTO particles exhibit the better dispersibility than TiO₂-LTO, whereas the agglomeration of TiO₂-LTO particles is more obvious. Moreover, in order to verify agglomeration tendency of the investigated LTO materials, the additional measurements have been carried out using the PSA technique, and these results are shown

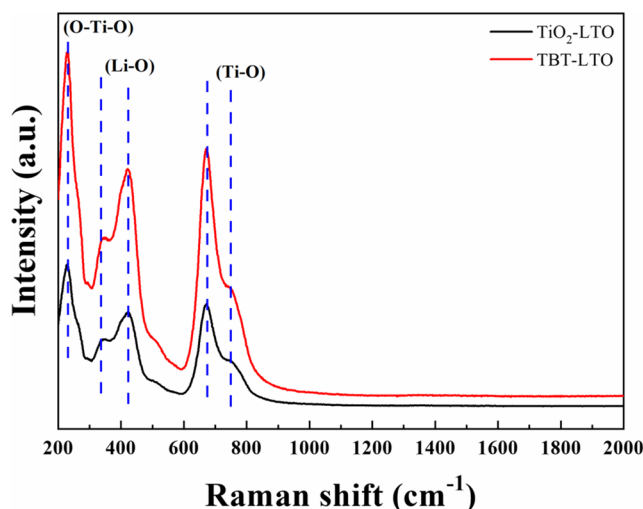


Fig. 2 Raman spectra of TiO₂-LTO and TBT-LTO

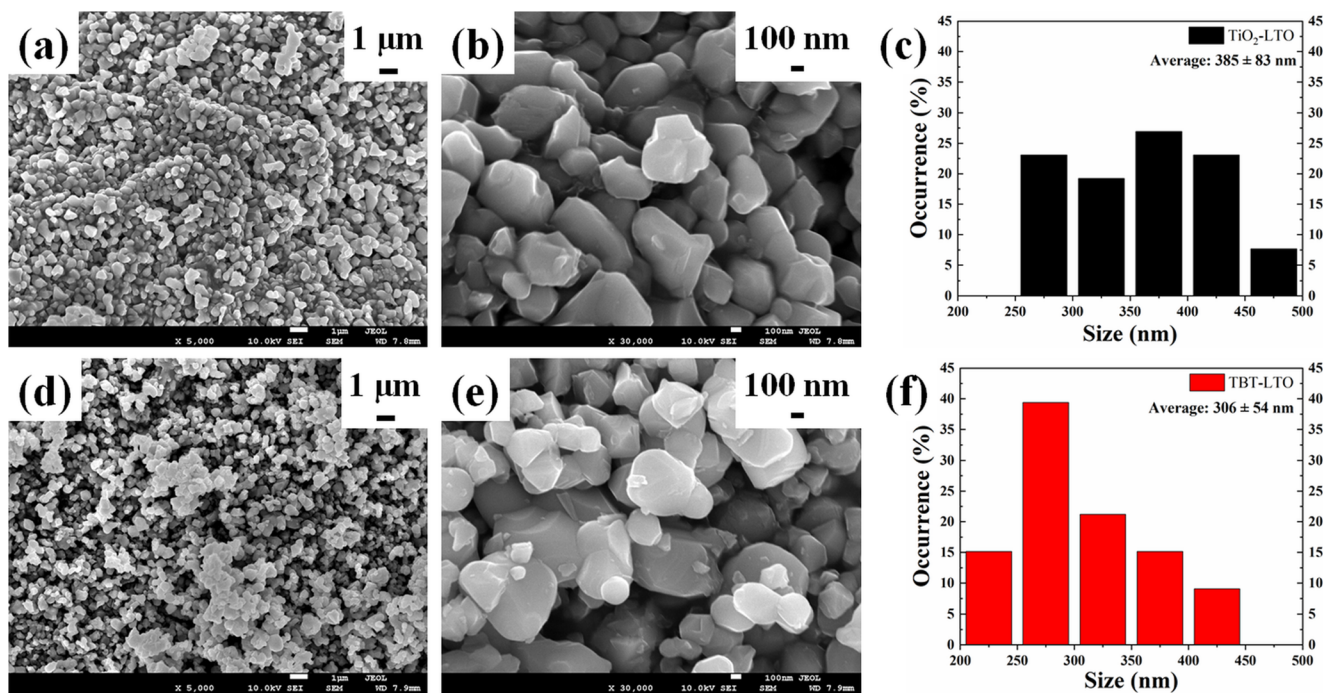


Fig. 3 SEM images at different magnifications and corresponding particle size distribution diagram of **a, b, c** TiO₂-LTO and **d, e, f** TBT-LTO

in Fig. S1. The average particle size of TiO₂ powder used as a titanium source is about 0.5 μm, and this value is greatly smaller than that obtained for TiO₂-LTO (8 μm) as shown in Fig. S1a and S1b, respectively. In turn, Fig. S1c and S1d present the distributions of particle sizes collected for the TBT precursor and the as-prepared TBT-LTO which, indeed, are similar. Moreover, the average particle size of TBT and TBT-LTO equals 2.96 μm and 3.04 μm, respectively. This surprising observation is associated with the fact that the TiO₂ particles are much smaller than the TBT precursor powder. Therefore, the smaller particles could agglomerate and form the well-packed structures which are easier to sinter during the synthesis process. This, in turn, caused the significant increase of TiO₂-LTO size in comparison with the size of TBT-LTO material. Further analysis of the magnified images shown in Fig. 3b and d allows determining that the average particles size of TiO₂-LTO (385 ± 83 nm) is larger than that of TBT-LTO (306 ± 54 nm). These results might be a bit confusing at the first moment because the values of particle size determined with this technique are much lower than that measured with PSA. Nevertheless, it is known that the PSA method does not provide the information whether the measured sizes are valid for agglomerations or single grains. Taking into account this important feature of PSA and the SEM results, it is supposed that both investigated LTO samples tend to agglomerate but the larger agglomerations are found for the TiO₂-LTO particles. This assumption is in good agreement with the BET results because the larger particles usually possess the lower surface area and vice versa. It is also important because the reduction of particle size can be beneficial for shortening the

transport of lithium-ion kinetics of lithium insertion/extraction into the LTO structure. Moreover, the previous literature reports have pointed out that the particle size significantly affects the electrochemical performance [12, 13, 31].

The charge and discharge curves recorded at various C-rates between 1.0 and 2.5 V vs. Li/Li⁺ for both LTO materials are shown in Fig. 4. Analyzing them, one can see that the flat charge and discharge plateau at an average potential of 1.55 V is clearly visible. This plateau corresponds to the Ti³⁺/Ti⁴⁺ redox processes which occur during the insertion/extraction of Li⁺ ions to spinel structure and at the same time corresponds to the reversible phase transition between spinel structure Li₄Ti₅O₁₂ and rock salt structure Li₇Ti₅O₁₂ (Li₄Ti₅O₁₂ + 3Li⁺ + 3e⁻ = Li₇Ti₅O₁₂; E = 1.55 V vs. Li/Li⁺ [6, 33–35]). The specific capacity at C-rates of 1, 5, and 10 C for TiO₂-LTO electrode is 120 mAh g⁻¹, 80 mAh g⁻¹, and 58 mAh g⁻¹, respectively, whereas the TBT-LTO electrode delivers specific capacity of 150 mAh g⁻¹, 120 mAh g⁻¹, and 63 mAh g⁻¹ at C-rates of 1, 5, and 10 C, respectively.

The cycling performance and coulombic efficiency for both LTO electrodes are shown in Fig. 5. According to the obtained data, the TiO₂-LTO as well as TBT-LTO electrode shows stable cycle life during the first 50 cycles. The coulombic efficiency contains between 98 and 100% and capacity retention displays the flat line after 50 cycles measured at various C-rates. This means that both electrode materials reveal good cycling performance. On the other hand, it is also important to note that the specific capacity for the TiO₂-LTO and TBT-LTO electrodes significantly decreases with the

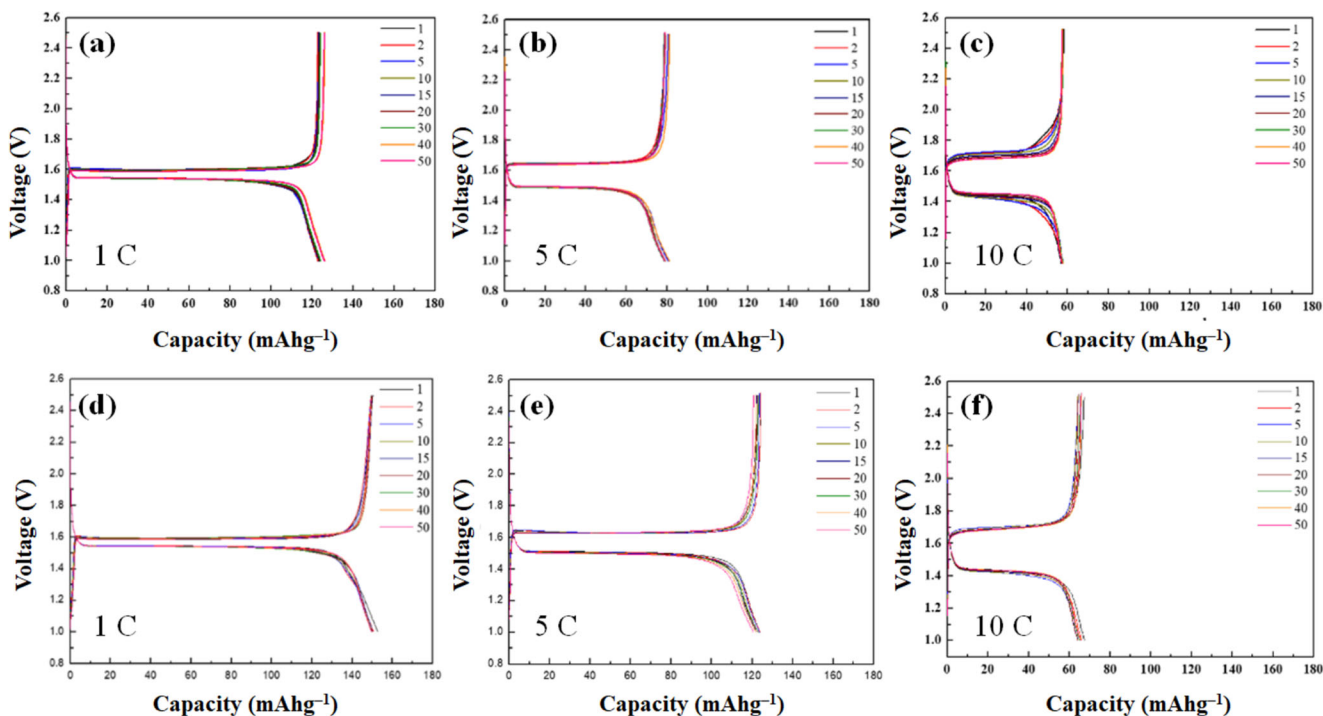


Fig. 4 Charge and discharge curves measured between 1.0 and 2.5 V vs. Li/Li⁺ for **a, b, c** TiO₂-LTO and **d, e, f** TBT-LTO at 1, 5, and 10 C, respectively; 1 C = 175 mA g⁻¹

increasing C-rate. In fact, this trend has been observed in the previous studies [16, 19, 30]. Nevertheless, the TBT-LTO electrode exhibits higher rate capability than the TiO₂-LTO electrode. This can be associated with its relatively lower size which offers more active electrode/electrolyte contact area, and, therefore, it results in shorter diffusion paths and better electrode reaction kinetics [5, 8, 12, 13, 36, 37].

Comparing the middle sections of the charge and discharge flat plateaus recorded at 1 C during the 10th cycle which are shown in Fig. 6, it is found that the interval between the charge and discharge curves is smaller for the TBT-LTO material (0.0511 V) than that of TiO₂-LTO (0.0596 V), and this is related to lower electrode polarization of the TBT-LTO electrode. Similar behavior has been observed in the case of CV

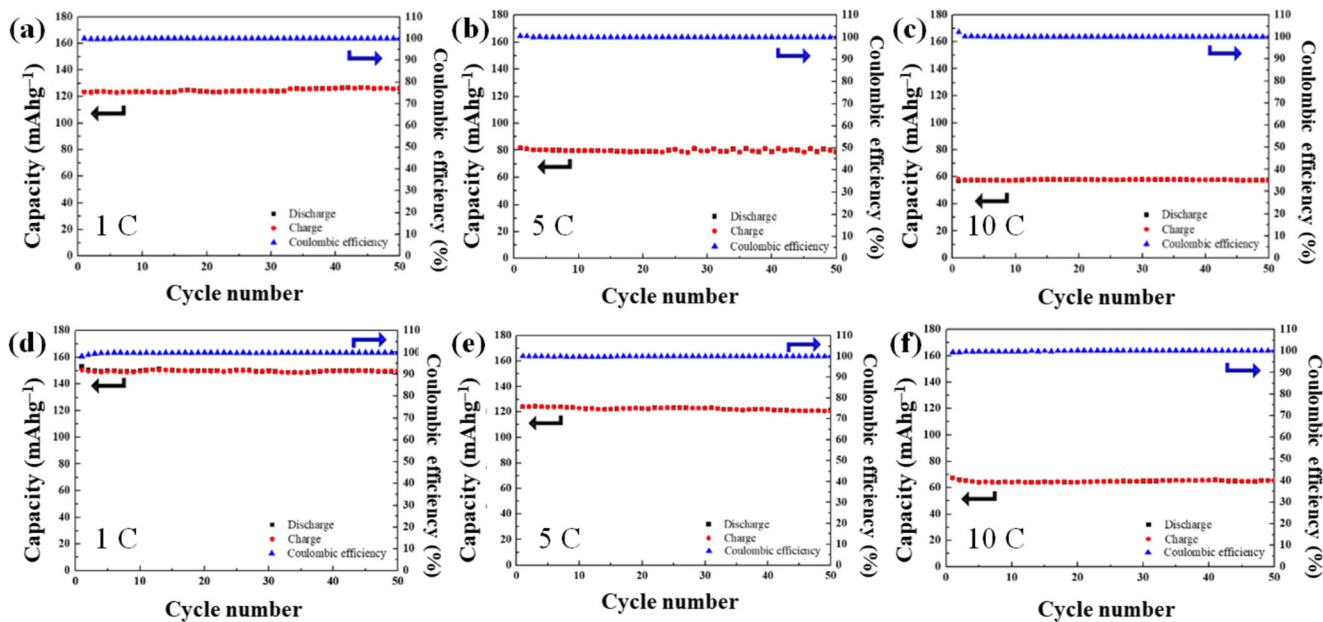


Fig. 5 Cycling performance and coulombic efficiency of **a, b, c** TiO₂-LTO and **d, e, f** TBT-LTO measured at 1, 5, and 10 C for 50 cycles, respectively; 1 C = 175 mA g⁻¹

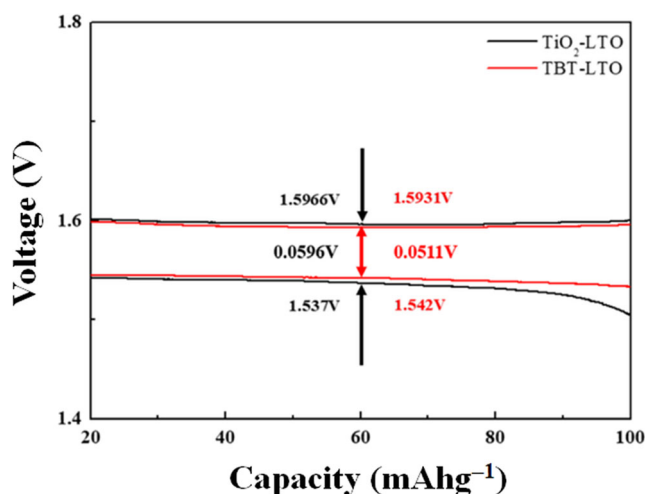


Fig. 6 Middle sections (20–100 mAh g⁻¹) of the charge/discharge plateaus recorded for TiO₂-LTO and TBT-LTO at 1 C during the 10th cycle

tests whose results are shown in Fig. 7. The differences between the anodic and cathodic peak potentials for TiO₂-LTO and TBT-LTO are about 0.162 V and 0.138 V, respectively. This indicates the higher degree of polarization for TiO₂-LTO sample [32]. Besides that, it is worth noting that the cyclic voltammograms of both LTO electrodes reveal only one pair of redox peaks which corresponds to oxidation and reduction processes of the Ti³⁺/Ti⁴⁺ couple. Those peaks are very sharp and fairly symmetrical, indicating an excellent reversibility of Li⁺ insertion/extraction in the LTO spinel and a fast kinetics of the electrochemical processes. However, based on the GCD and CV experiments, it is clear that the TBT-LTO electrode exhibits better kinetics properties. Finally, it should be also noted that the peak area under CV obtained for the TiO₂-LTO was smaller than that of TBT-LTO. This confirms that the TBT-LTO anode material reveals higher reversibility as

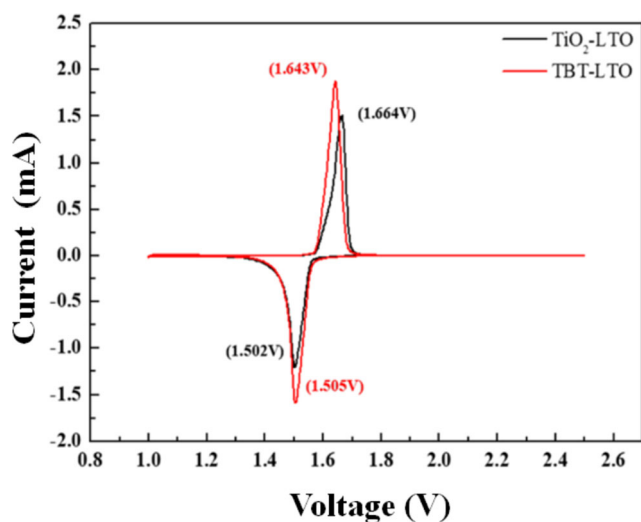


Fig. 7 Cyclic voltammetry of TiO₂-LTO and TBT-LTO in the voltage window of 1.0–2.5 V and at the scanning rate of 0.1 mV s⁻¹

well as capacity, and it is in good agreement with the results derived from GCD tests.

The EIS measurements were performed after 10 cycles of CV in order to illustrate the different electrochemical impedance and electronic conductivity for both LTO samples. The Nyquist plots recorded for the LTO electrodes and their equivalent circuit model are shown in Fig. 8a. The plots are composed of two partially overlapping semicircles and one slope line. In turn, the equivalent circuit comprises of several components, i.e., R_s —resistance of electrolyte, R_{int} and CPE1—resistance of polarization and surface capacitance at high frequency, respectively, R_{ct} and CPE2—the charge transfer resistance (electronic and ionic conductivity) and double-layer capacitance of the electrode recorded at medium frequency, respectively, and W —Warburg impedance recorded at a low frequency and caused by Li⁺ diffusion in the electrode material [29, 34, 36]. The simulated results for the EIS measurements are collected in Table 1. Analyzing them, one can see

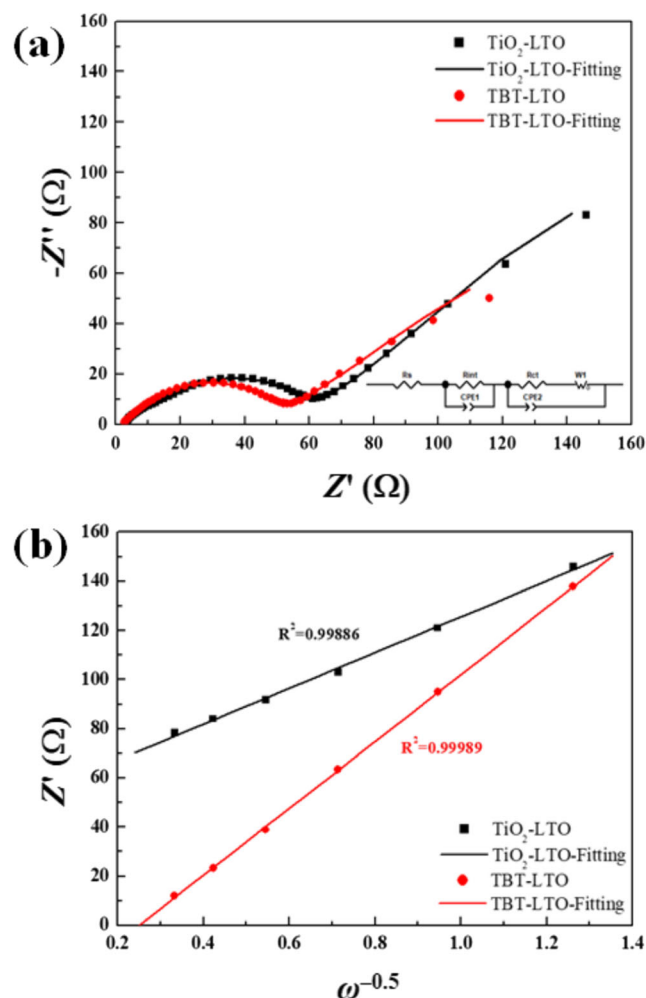


Fig. 8 **a** EIS results for TiO₂-LTO and TBT-LTO electrodes recorded with the frequency range of 10⁻²–10⁶ Hz after 10 cycles at 0.1 mV of CV spectra. **b** Real part component of the impedance spectrum vs. $\omega^{-0.5}$ at the low-frequency region for TiO₂-LTO and TBT-LTO

Table 1 Values of resistance of electrolyte (R_s), polarization resistance (R_{int}), charge transfer resistance (R_{ct}), Warburg impedance coefficient (σ), and Li^+ diffusion coefficient (D)

Sample	R_s (Ω)	R_{int} (Ω)	R_{ct} (Ω)	σ ($\text{W s}^{-0.5}$)	D ($\text{cm}^2 \text{s}^{-1}$)
TiO ₂ -LTO	2.96	10.31	46.16	72.84	5.7×10^{-13}
TBT-LTO	2.38	4.17	43.13	55.41	9.8×10^{-13}

that the R_s , R_{int} , and R_{ct} values obtained for TBT-LTO are smaller than that for TiO₂-LTO. This can be explained taking into account the smaller particle size of the TBT-LTO sample which influences the electronic conductivity and the kinetic behavior. In order to confirm this statement, the Li^+ diffusion coefficient was calculated by using the following equations:

$$Z_{re} = R_s + R_{ct} + \sigma\omega^{-0.5} \quad (1)$$

$$D = (R^2 T^2) / (2A^2 n^4 F^4 C^2 \sigma^2) \quad (2)$$

where D is the Li^+ diffusion coefficient, R is the gas constant ($8.314 \text{ J mol}^{-1} \text{ K}^{-1}$), T is the room temperature (298 K), A is the surface area of the electrode (0.785 cm^2), n is the number of electrons during the half reaction of the redox couple (equal to 1), F is the Faraday constant ($96,500 \text{ C mol}^{-1}$), C is the molar concentration of Li^+ in solid ($4.37 \times 10^{-3} \text{ mol cm}^{-3}$), σ is the Warburg impedance coefficient, and ω is the angular frequency. The values of constant parameters have been taken from the previous literature [6, 13, 33], whereas the σ coefficient is calculated through Eq. 1 from the slope lines between Z_{re} (real part of the impedance) and $\omega^{-0.5}$ shown in Fig. 8b. This allows estimating the value of Li^+ diffusion coefficient from Eq. 2. Both calculated D and σ values are also placed in Table 1, and they prove that the TBT-LTO material has higher Li^+ diffusion coefficient than the TiO₂-LTO sample. This agrees well with our assumption that the reduced particle size enhances the Li^+ diffusion. Moreover, this indicates the improvement of the Li^+ ion kinetic which facilitates the charge transfer reactions during charge and discharge processes.

Conclusions

The two LTO anode materials have been successfully prepared by the sol-gel method with the use of different titanium sources, i.e., tetrabutyl titanate and titanium dioxide. According to the obtained XRD and Raman spectroscopy results, the TBT-LTO sample possesses better dispersibility and smaller particle size than that of TiO₂-LTO material. We also indicate that these features affect the lower polarization phenomenon and higher lithium-ion diffusion coefficient for the TBT-LTO electrode material. As a result, the TiO₂-LTO electrode delivers 120 mAh g^{-1} , 80 mAh g^{-1} , and

58 mAh g^{-1} , whereas the specific capacity of the TBT-LTO electrode is 150 mAh g^{-1} , 120 mAh g^{-1} , and 63 mAh g^{-1} measured at C-rate of 1, 5, and 10 C, respectively. Even though the values of specific capacity vary for both investigated LTO samples, it is found that their capacity retentions do not differ significantly and their Coulombic efficiencies reach almost 100% after 50 cycles. Concluding, the results presented in this work indicate that the choice of titanium source in the synthesis of $\text{Li}_4\text{Ti}_5\text{O}_{12}$ material influences its morphological properties as well as electrochemical performance.

Acknowledgments The authors acknowledge Ms. Su-Jen Ji from the Ministry of Science and Technology for the assistance in the FE-SEM experiments.

Contributor roles taxonomy Chung-Yuan Kang: Data curation, investigation, writing—original draft.

Marcin Krajewski: Data curation, methodology, visualization, writing—review and editing.

Jeng-Yu Lin: Conceptualization, formal analysis, funding acquisition, methodology, supervision, writing—review and editing.

Funding The authors would like to appreciate the Ministry of Science and Technology Taiwan for the financial support (Project numbers: MOST 108-3116-F-036-001 and MOST 106-2923-E-036-002-MY3).

Compliance with ethical standards

Conflict of interest The authors declare that they have no conflict of interest.

Open Access This article is licensed under a Creative Commons Attribution 4.0 International License, which permits use, sharing, adaptation, distribution and reproduction in any medium or format, as long as you give appropriate credit to the original author(s) and the source, provide a link to the Creative Commons licence, and indicate if changes were made. The images or other third party material in this article are included in the article's Creative Commons licence, unless indicated otherwise in a credit line to the material. If material is not included in the article's Creative Commons licence and your intended use is not permitted by statutory regulation or exceeds the permitted use, you will need to obtain permission directly from the copyright holder. To view a copy of this licence, visit <http://creativecommons.org/licenses/by/4.0/>.

References

- Friedrichs J (2010) Global energy crunch: how different parts of the world would react to a peak oil scenario. *Energy Policy* 38(8): 4562–4569
- Mitchell T (2010) The resources of economics. *J Cult Econ* 3(2): 189–204
- Hall PJ, Bain EJ (2008) Energy-storage technologies and electricity generation. *Energy Policy* 36(12):4352–4355
- Xie ZW, Li X, Li W, Chen MZ, Qu MZ (2015) Graphene oxide/lithium titanate composite with binder-free as high capacity anode material for lithium-ion batteries. *J Power Sources* 273:754–760

5. Cao N, Song ZH, Liang Q, Gao XJ, Qin X (2017) Hierarchical $\text{Li}_4\text{Ti}_5\text{O}_{12}/\text{C}$ composite for lithium-ion batteries with enhanced rate performance. *Electrochim Acta* 235:200–209
6. Wang DD, Shan ZQ, Tian JH, Chen Z (2019) Understanding the formation of ultrathin mesoporous $\text{Li}_4\text{Ti}_5\text{O}_{12}$ nanosheets and their application in high-rate, long-life lithium-ion anodes. *Nanoscale* 11(2):520–531
7. Bonnisa Magdaline T, Vadivel Murugan A (2020) Microwave-assisted hydrometallurgical extraction of $\text{Li}_4\text{Ti}_5\text{O}_{12}$ and LiFePO_4 from ilmenite: effect of PPy-Br₂ derived C-coating with N, Br, and Nb⁵⁺ Co-doping on electrodes for high-rate energy storage performance. *Dalton Trans* 49(19):6227–6241
8. Michalska M, Krajewski M, Ziolkowska D, Hamankiewicz B, Andrzejczuk M, Lipinska L, Korona KP, Czerwinski A (2014) Influence of milling time in solid-state synthesis on structure, morphology and electrochemical properties of $\text{Li}_4\text{Ti}_5\text{O}_{12}$ of spinel structure. *Powder Technol* 266:372–377
9. Pang SP, Zhao YY, Zhang CJ, Zhang QH, Gu L, Zhou XH, Li GC, Cui GL (2013) Electrostatic assembly of mesoporous $\text{Li}_4\text{Ti}_5\text{O}_{12}/$ graphene hybrid as high-rate anode materials. *Scr Mater* 69(2):171–174
10. Wang J, Liu XM, Yang H, Shen XD (2011) Characterization and electrochemical properties of carbon-coated $\text{Li}_4\text{Ti}_5\text{O}_{12}$ prepared by a citric acid sol–gel method. *J Alloys Compd* 509(3):712–718
11. Kashkooli AG, Lui G, Farhad S, Lee DU, Feng K, Yu AP, Chen ZW (2016) Nano-particle size effect on the performance of $\text{Li}_4\text{Ti}_5\text{O}_{12}$ spinel. *Electrochim Acta* 196:33–40
12. Pohjalainen E, Rauhala T, Valkeapää M, Kallioinen J, Kallio T (2015) Effect of $\text{Li}_4\text{Ti}_5\text{O}_{12}$ particle size on the performance of lithium ion battery electrodes at high C-rates and low temperatures. *J Phys Chem C* 119(5):2277–2283
13. Wang D, Wu XY, Zhang YY, Wang J, Yan P, Zhang CM, He DN (2014) The influence of the TiO_2 particle size on the properties of $\text{Li}_4\text{Ti}_5\text{O}_{12}$ anode material for lithium-ion battery. *Ceram Int* 40:3799–3804
14. Chen CH, Vaughney JT, Jansen AN, Dees DW, Kahaian AJ, Goacher T, Thackeray MM (2001) Studies of Mg-substituted $\text{Li}_{4-x}\text{Mg}_x\text{Ti}_5\text{O}_{12}$ spinel electrodes ($0 \leq x \leq 1$) for lithium batteries. *J Electrochem Soc* 148(1):A102–A104
15. Jhan YR, Lin CY, Duh JG (2011) Preparation and characterization of ruthenium doped $\text{Li}_4\text{Ti}_5\text{O}_{12}$ anode material for the enhancement of rate capability and cyclic stability. *Mater Lett* 65(15–16):2502–2505
16. Yu ZJ, Zhang XF, Yang GL, Liu J, Wang JW, Wang RS, Zhang JP (2011) High rate capability and long-term cyclability of $\text{Li}_4\text{Ti}_{4.9}\text{V}_{0.1}\text{O}_{12}$ as anode material in lithium ion battery. *Electrochim Acta* 56(24):8611–8617
17. Lin CF, Ding B, Xin YL, Cheng FQ, Lai MO, Lu L, Zhou HH (2014) Advanced electrochemical performance of $\text{Li}_4\text{Ti}_5\text{O}_{12}$ -based materials for lithium-ion battery: synergistic effect of doping and compositing. *J Power Sources* 248:1034–1041
18. Zhang B, Du HD, Li BH, Kang FY (2010) Structure and electrochemical properties of Zn-doped $\text{Li}_4\text{Ti}_5\text{O}_{12}$ as anode materials in Li-ion battery. *Electrochem Solid-State Lett* 13(4):A36–A38
19. Yang GJ, Park SJ (2020) Single-step solid-state synthesis and characterization of $\text{Li}_4\text{Ti}_{5-x}\text{Fe}_x\text{O}_{12-y}$ ($0 \leq x \leq 0.1$) as an anode for lithium-ion batteries. *J Mater Chem A* 8(5):2627–2636
20. Qi YL, Huang YD, Jia DZ, Bao SJ, Guo ZP (2009) Preparation and characterization of novel spinel $\text{Li}_4\text{Ti}_5\text{O}_{12-x}\text{Br}_x$ anode materials. *Electrochim Acta* 54(21):4772–4776
21. Luo HJ, Shen LF, Rui K, Li HS, Zhang XG (2013) Carbon coated $\text{Li}_4\text{Ti}_5\text{O}_{12}$ nanorods as superior anode material for high rate lithium ion batteries. *J Alloys Compd* 572:37–42
22. Chang CM, Chen YC, Ma WL, Wang PH, Lee CF, Chen HS, Chen-Yang YW (2015) Sol–gel synthesis of low carbon content and low surface area $\text{Li}_4\text{Ti}_5\text{O}_{12}/$ carbon black composites as high-rate anode materials for lithium ion batteries. *RSC Adv* 5(91):74381–74390
23. Kuo YC, Lin JY (2014) One-pot sol-gel synthesis of $\text{Li}_4\text{Ti}_5\text{O}_{12}/\text{C}$ anode materials for high-performance Li-ion batteries. *Electrochim Acta* 142:43–50
24. Hong SA, Lee SB, Joo OS, Kang JW, Cho BW, Lim JS (2016) Synthesis of lithium titanium oxide ($\text{Li}_4\text{Ti}_5\text{O}_{12}$) with ultrathin carbon layer using supercritical fluids for anode materials in lithium batteries. *J Mater Sci* 51(13):6220–6234
25. Li W, Li X, Chen MZ, Xie ZW, Zhang JX, Dong SQ, Qu MZ (2014) AlF_3 modification to suppress the gas generation of $\text{Li}_4\text{Ti}_5\text{O}_{12}$ anode battery. *Electrochim Acta* 139:104–110
26. Li X, Lin HC, Cui WJ, Xiao Q, Zhao JB (2014) Fast solution-combustion synthesis of nitrogen-modified $\text{Li}_4\text{Ti}_5\text{O}_{12}$ nanomaterials with improved electrochemical performance. *ACS Appl Mater Interfaces* 6(10):7895–7901
27. Liu W, Wang Q, Zhang J, Xie XH, Liu HH, Min GQ, Xia BJ (2016) Isothermal kinetic analysis of the effects of high-energy ball milling on solid-state reaction of $\text{Li}_4\text{Ti}_5\text{O}_{12}$. *Powder Technol* 287:373–379
28. Ning F, He YB, Li BH, Du HD, Zhai DY, Kang FY (2012) Effects of TiO_2 crystal structure on the performance of $\text{Li}_4\text{Ti}_5\text{O}_{12}$ anode material. *J Alloys Compd* 513:524–529
29. Wu FX, Li XH, Wang ZX, Guo HJ, Wu L, Xiong XH, Wang XJ (2011) Preparation of TiO_2 nanosheets and $\text{Li}_4\text{Ti}_5\text{O}_{12}$ anode material from natural ilmenite. *Powder Technol* 213(1–3):192–198
30. Chen MM, Sun X, Qiao ZJ, Ma QQ, Wang CY (2014) Anatase- TiO_2 nanocoating of $\text{Li}_4\text{Ti}_5\text{O}_{12}$ nanorod anode for lithium-ion batteries. *J Alloys Compd* 601:38–42
31. Wang JS, Wang BF, Cao J, Tang YF (2014) Facile solution-based synthesis of spinel $\text{Li}_4\text{Ti}_5\text{O}_{12}$ nanosheets and the application in lithium ion batteries. *Solid State Ionics* 268:131–134
32. Vikram Babu B, Vijaya Babu K, Tewodros Aregai G, Seeta Devi L, Madhavi Latha B, Sushma Reddi M, Samatha K, Veeraiah V (2018) Structural and electrical properties of $\text{Li}_4\text{Ti}_5\text{O}_{12}$ anode material for lithium-ion batteries. *Results Phys* 9:284–289
33. Zhang P, Huang YD, Jia W, Cai YJ, Wang XC, Guo Y, Jia DZ, Sun ZP, Wang RY, Tang XC, Wang LS (2016) High rate capability of lithium chromium titanium oxide hierarchical mesoporous microspheres anode materials synthesized by a one-pot co-precipitation for lithium ion batteries. *J Electrochem Soc* 163:A1920–A1926
34. Erdas A, Ozcan S, Nalci D, Guler MO, Akbulut H (2015) Novel $\text{Ag}/\text{Li}_4\text{Ti}_5\text{O}_{12}$ binary composite anode electrodes for high capacity Li-ion batteries. *Surf Coatings Technol* 271:136–140
35. Hirayama M, Kim K, Toujigamori T, Cho W, Kanno R (2011) Epitaxial growth and electrochemical properties of $\text{Li}_4\text{Ti}_5\text{O}_{12}$ thin-film lithium battery anodes. *Dalton Trans* 40(12):2882–2887
36. Zhang CM, Zhang YY, Wang J, Wang D, He DN, Xia YY (2013) $\text{Li}_4\text{Ti}_5\text{O}_{12}$ prepared by a modified citric acid sol–gel method for lithium-ion battery. *J Power Sources* 236:118–125
37. Wang J, Zhao HL, Li ZL, Wen YT, Xia Q, Zhang Y, Yushin G (2016) Revealing rate limitations in nanocrystalline $\text{Li}_4\text{Ti}_5\text{O}_{12}$ anodes for high-power lithium ion batteries. *Adv Mater Interfaces* 1600003:1–8

Publisher's note Springer Nature remains neutral with regard to jurisdictional claims in published maps and institutional affiliations.